

Brushless AC Interior-Permanent Magnet Motor Design: Comparison of Slot/Pole Combinations and Distributed Vs. Concentrated Windings

James Goss, Dave Staton
Motor Design Limited
Ellesmere, UK
james.goss@motor-design.com

Rafal Wrobel, Phil Mellor
Department of Electrical & Electronic Engineering
University of Bristol, UK

Abstract-- This paper compares the attributes of 36 slot, 33 slot and 12 slot brushless interior permanent magnet motor designs, each with an identical 10 pole interior magnet rotor. The aim of the paper is to quantify the trade-offs between alternative distributed and concentrated winding configurations taking into account aspects such as thermal performance, field weakening behaviour, acoustic noise, and efficiency. It is found that the concentrated 12 slot design gives the highest theoretical performance however significant rotor losses are found during testing and a large amount of acoustic noise and vibration is generated. The 33 slot design is found to have marginally better performance than the 36 slot but it also generates some unbalanced magnetic pull on the rotor which may lead to mechanical issues at higher speeds.

I. INTRODUCTION

Interior permanent magnet motors (IPM) are an appealing prospect in traction applications due to their high torque density and good field weakening performance enabling a wide speed range. Two crucial aspects of any design are the slot/pole combination and the choice between a distributed and concentrated winding configuration. In this paper the performances of three IPM motors designed for an electric vehicle application are compared. Each motor has an identical 10 pole rotor; while 12, 33 and 36 slot stators are compared in terms of torque and power density, efficiency, field weakening performance, continuous thermally constrained operating envelopes, torque ripple, acoustic noise and vibration.

A comparison between distributed and concentrated winding topologies has been undertaken a number of times in the literature. The main advantage of concentrated windings is lower winding resistance due to shorter end turns and typically a higher slot fill factor [1]. Fractional slot

concentrated windings are also found to provide a higher inductance which is advantageous when designing for a wide speed range [2]. However a reduction in the saliency ratio occurs with concentrated windings in an IPM machine when compared to an equivalent distributed winding. Concentrated windings can generate sub-harmonic MMF components that result in significant additional rotor core and magnet losses at high speed [1], [3]. High levels of acoustic noise and vibration have also been associated with certain fractional slot pole-slot combinations, particularly 12 slot 10 pole, due to low order vibration modes [4], [5].

The choice of slot/pole combination has also been discussed in detail [6],[7]. An increase in the number of poles results in increased torque/amp capability as well as increased fundamental frequency of the current waveform, thus a trade-off exists between low speed and high speed power losses [8]. The number of slots is typically chosen based upon the fundamental winding factor (k_{w1}) and the lowest common multiple (LCM) between the number of poles and slots. The winding factor provides a measure of the utilization of the air-gap flux and hence directly affects the torque constant while the LCM gives the number of cogging periods per mechanical revolution; a high LCM suggests a low cogging torque amplitude.

In this paper 36, 33 and 12 slot, 10 pole IPM motor designs are compared, based around a common rotor design. The 12 slot design uses a concentrated double layered winding configuration, while the 33 and 36 slot designs adopt a distributed double layer winding. Each motor has the same active length, active diameter and stator diameter and each is designed to meet the same performance specification

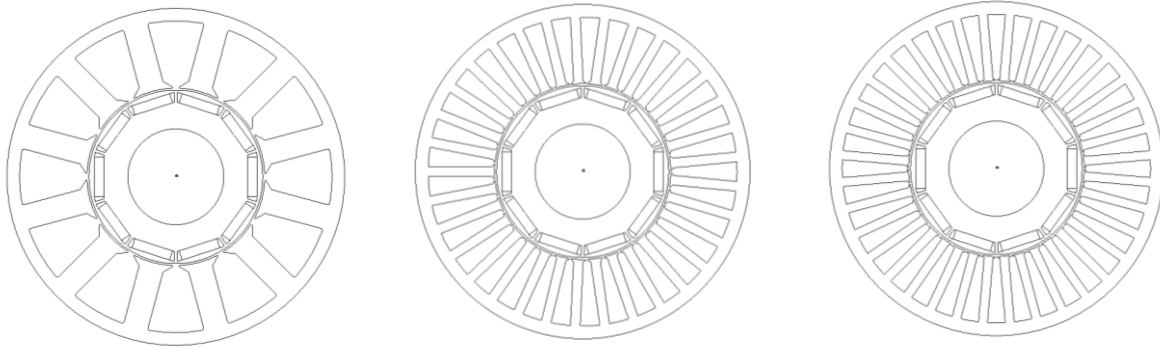


Figure 1. 12, 33 and 36 slot design cross-section

II. MOTOR DESIGNS AND EXPERIMENTAL CALIBRATION

The three machine variants have been designed against a set of requirements typical of a small electric vehicle propulsion system. The specification and common design parameters are shown in table I and II respectively.

TABLE I - SPECIFICATION

DC Link Voltage (V)	240
Maximum Inverter Current (A_{pk})	250
Low Speed Continuous Torque (Nm)	30
High Speed Continuous Power (kW)	12
Peak Torque Requirement (Nm)	60
Peak Power Requirement (kW)	20

TABLE II - COMMON DESIGN PARAMETERS

Stator Outer Diameter (mm)	175
Stack Length (mm)	90
Magnet Grade	N38UH
Electrical Steel Grade	M270-35A
Open Circuit Stator Tooth Flux Density (T)	1.2
Open Circuit Stator Yoke Flux Density (T)	1.2
Maximum Speed (rpm)	10,000
Slot Fill Factor	0.45

The common IPM rotor, fig. 2, is designed to a magnetic loading of 0.75T. The stator laminations are sized for a peak open circuit flux density equal to 1.2T in the tooth and back iron on open circuit. The stack length is 90mm. The stator designs have been optimised against the performance requirements using the procedure described in [9] and the ensuing lamination design for each motor is shown in fig.1.

At the time of publication only the 12 slot design has been built and tested although it is planned to prototype and test all three variants. The test rig arrangement is shown in Fig. 4. A load machine is coupled to the machine under test (MUT) and operated in speed control mode. The MUT can be reconfigured to run at open circuit and short circuit

conditions or on load motoring operation when connected to a drive and operated in torque control mode.

The test results have been used to validate the electromagnetic and thermal models as well as measuring various loss components. As would be expected the match between the electromagnetic FEA and test data is very good, with an accurate back-emf waveform shape and magnitude as shown in fig. 3. The various loss components have been separated using open and short-circuit tests and these along with a static DC test have been used to calibrate the lumped parameter thermal model.



Figure 2. Fabricated rotor

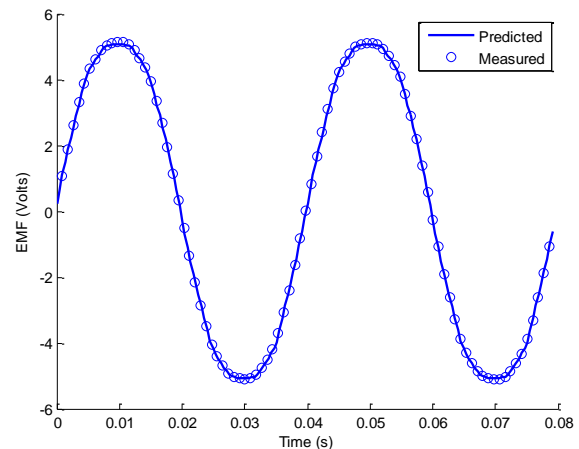


Figure 3. Measured and predicted back-emf waveform at 300rpm

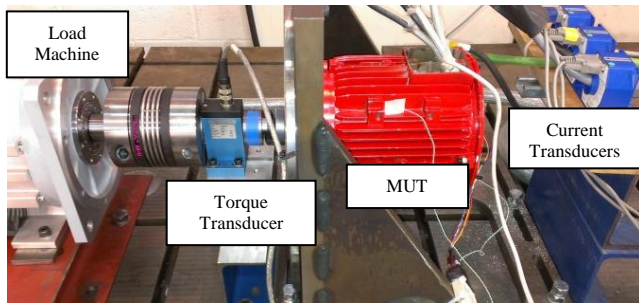


Figure 4. Test rig arrangement

III. ELECTROMAGNETIC PERFORMANCE COMPARISON

TABLE III-ELECTROMAGNETIC PARAMETERS

	12 Slot	33 Slot	36 Slot
k_{w1}	0.933	0.9456	0.9236
LCM	60	330	180
λ_m (mWb)	32.4	37.4	39.9
L_d (mH)	0.29	0.27	0.29
L_q (mH)	0.42	0.46	0.50
Saliency Ratio	1.46	1.69	1.72
Isc (A_{pk})	112	138	139
Turns/Phase	28	33	36
Iron (kg)	8.5	8.8	8.8
Copper (kg)	5.2	6.2	5.9

A well-known characteristic of concentrated windings is that they tend to exhibit a higher inductance when compared to a distributed winding that links equivalent magnet flux; concentrated windings have also been shown to have a detrimental effect on the saliency ratio of the machine. Table III confirms these findings; the result of the higher ratio of permanent magnet flux linkage to inductance as well as a reduced saliency ratio in the concentrated machine is a lower short circuit or characteristic current. An optimal constant power speed range occurs when the short circuit current is equal to the rated current. Here this design aim is more easily achieved with the concentrated winding and the measured short circuit current of $112A_{pk}$ corresponds to a current density of $3.7A_{rms}/mm^2$ in the phase windings while the short circuit current of the distributed machines, $138A_{pk}$ for the 33 slot and $139A_{pk}$ for the 36 slot, correlates to a current density of $5.4A_{rms}/mm^2$ and $5.9A_{rms}/mm^2$ respectively, slightly high for a design with no forced cooling.

The peak power capability of a PM machine in the field weakening region is determined by the specific value of the short circuit current and the maximum supply voltage. The number of turns for each machine has been chosen to meet

the required peak torque within the limit of the inverter current while also maximising peak power in the field weakening region. This trade-off between torque per amp at low speed and peak power at high speed is more difficult to achieve with a lower ratio of PM flux linkage to d-axis inductance and hence the concentrated winding machine has a reduced peak performance envelope when compared to the distributed machines, fig. 5.

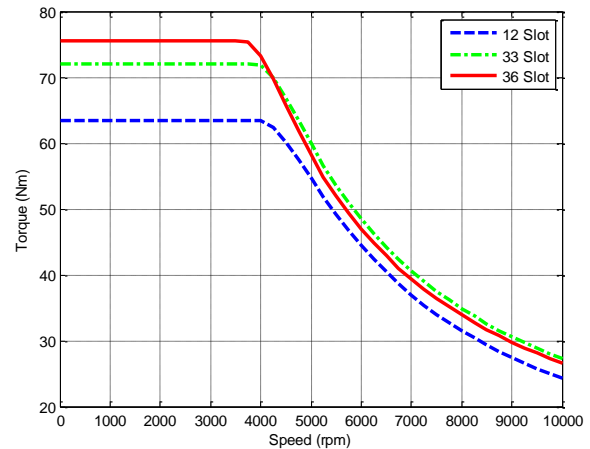


Figure 5. Peak performance envelope with a $250A_{pk}$ inverter current limit

Table IV shows torque production at the maximum torque/amp (MTPA) operating point and a current density of $4A_{rms}/mm^2$. The automated tooth and slot depth sizing process was found to result in a lower required quantity of stator iron in the 12 slot, Table III, and hence a larger total available slot area, when compared to the distributed designs. The consequence of this is that for a given current density and equivalent slot fill factor the concentrated winding is able to produce a higher torque despite a reduced saliency ratio and consequent lower amount of reluctance torque. The 33 slot produces a higher torque than the 36 slot due to its larger fundamental winding factor.

TABLE IV-TORQUE PRODUCTION AT RATED CURRENT

	12 Slot	33 Slot	36 Slot
Torque at $4A/mm^2$ (Nm)	34.5	32.9	31.7
Current Angle for MTPA ($^\circ$)	15.5	20	20

While all three designs have relatively similar fundamental winding factors, fig. 6, the 33 slot 10 pole combination gives the highest. Consequently along with its large value of the LCM between the poles and slots the 33-slot configuration makes an attractive choice. However this pole/slot combination exhibits a small amount of unbalanced magnetic pull which may result in a higher level of vibration and additional mechanical stress on the bearings creating extra losses at high speed. The higher order

winding factors show relatively small 5th and 7th components for all designs and larger 9th and 11th components for the 12 slot design.

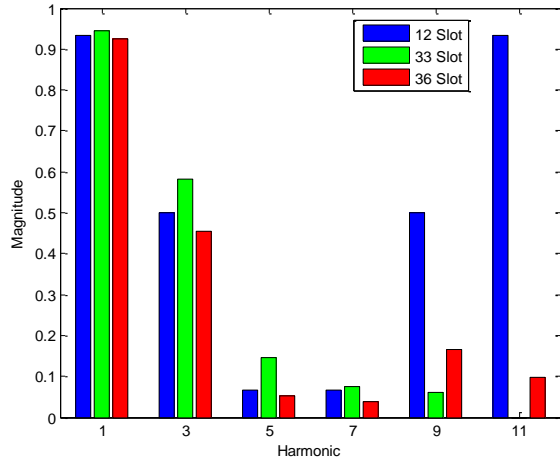


Figure 6. Winding factors

Fig. 7 shows the harmonic content of the predicted back-emf waveform for each design with each component normalised to the fundamental. The waveforms are very sinusoidal; the 3rd harmonic component is the largest however this is suppressed by the winding star connection and hence has no impact on performance. The 12 slot design has the highest 5th and 11th harmonic, while the 33 slot has the largest 7th.

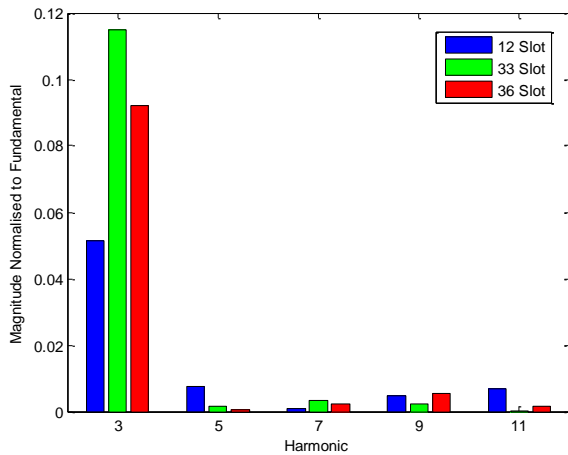


Figure 7. Harmonic content of back-emf waveform

IV. LOSS COMPARISON

Table V. shows the predicted DC copper loss for each machine at rated current density of $4A/mm^2$ and the iron loss at 10,000 rpm for open and short circuit conditions with a build factor of 2 to allow for any degradation in the material properties during the stamping and assembly of the lamination pack. The copper loss is lowest for the concentrated winding due to the shorter end turns and the 33

has slightly higher copper loss when compared to the 36 slot as the span of the end windings is slightly larger. While there is more rotor loss in the concentrated design the overall level of iron loss at both short circuit and open circuit is the lowest and the 36 slot shows slightly higher iron loss than the 33 slot.

TABLE V-DC COPPER AND IRON LOSS COMPARISON

	12 Slot	33 Slot	36 Slot
DC Copper Loss at $4A/mm^2$ (W)	211.8	252.3	240.6
Stator OC Iron Loss (W)	402.8	514.6	523.6
Rotor OC Iron Loss (W)	5.6	0.5	0.5
Stator SC Iron Loss (W)	213.8	294.4	316.5
Rotor SC Iron Loss (W)	61.4	39.1	42.8

The additional loss components in the 12 slot have been measured using open and short circuit tests up-to speeds of 4000rpm and separated based on the relationship of the various components of loss with frequency as well as the measured temperature rise in various parts of the machine during the test procedure when compared to a calibrated thermal model.

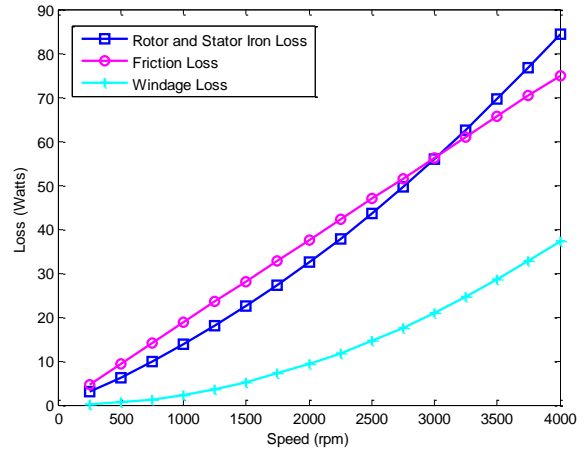


Figure 8. Measured open circuit losses

Fig. 8 shows the measured open circuit power losses for the 12 slot motor divided into friction, windage and iron loss components. The iron loss at each measurement point has been estimated from a finite element field solution over an electrical cycle and multiplied by a build factor of 2. The friction loss is attributed to the front and rear bearings, this is a significant component of the loss and results in a large temperature rise around the bearings in the open circuit test.

Fig. 9 plots the total measured loss at short circuit. In addition the figure shows stator winding ohmic losses calculated from the measured rms current and the temperature winding resistance. This copper loss component has been calculated in order to separate out frequency

dependent loss effects. The DC copper loss component falls slightly with increasing speed as the short circuit current reduces due to increasing magnet temperature. The components that make up the frequency dependant loss are considered in fig. 10. Here the iron loss has been estimated in the same manner as the open circuit results and the friction and windage components were taken from the open circuit measurements, fig. 8. There is also some AC winding loss due to eddy current, skin and proximity effects as well as a significant component of rotor loss attributed to the magnets. The AC winding loss and rotor loss components have been split through comparison of a calibrated lumped-parameter thermal model and the measured temperature rise throughout the test procedure. This additional loss in the rotor appears to scale with the square of the frequency and similar effects have been found with the use of concentrated windings previously [1].

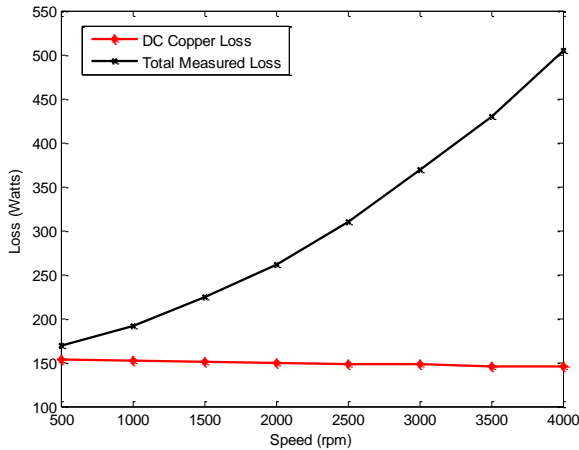


Figure 9. Measured Total and DC Copper Loss at short circuit

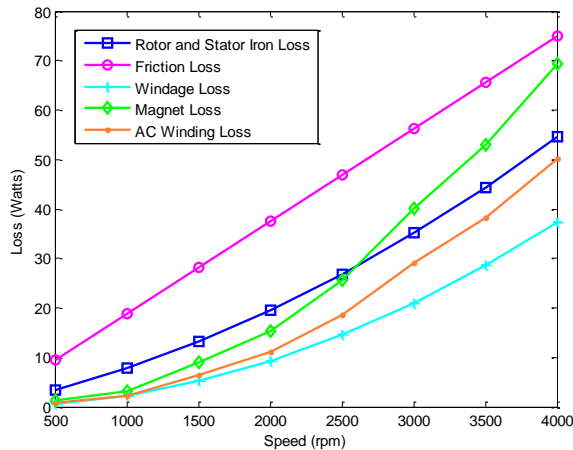


Figure 10. Split of Additional Loss components at short circuit

Fig.11 shows an calculated efficiency map of the 12 slot design, developed using the techniques described in [10] and the various loss components calibrated from the test results. The peak efficiency region of 96% is found at 2000-

3000rpm and 20-30Nm. However the efficiency falls at higher speeds due to the various frequency related loss components.

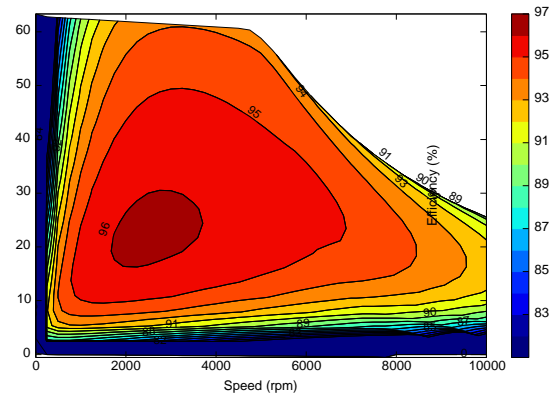


Figure 11. Calibrated efficiency map of the 12 slot design

V. THERMAL PERFORMANCE

Table VI shows the distribution of temperatures across the slot with 400W of copper loss in the winding calculated using a 2D thermal FEA model, fig. 12. Here it can be seen that while the 33 and 36 slot windings have very similar temperatures the hotspot and average temperatures in the 12 slot are higher due to the wider slots resulting in a larger hotspot to housing thermal resistance. Therefore the higher losses in the distributed windings are mitigated by improved thermal performance.

TABLE VI-COMPARISON OF WINDING TEMPERATURES CALCULATED USING 2D THERMAL FEA

	12 Slot	33 Slot	36 Slot
Winding Minimum (°C)	116	116	116
Winding Average (°C)	121	118	117
Winding Hotspot (°C)	126	120	120

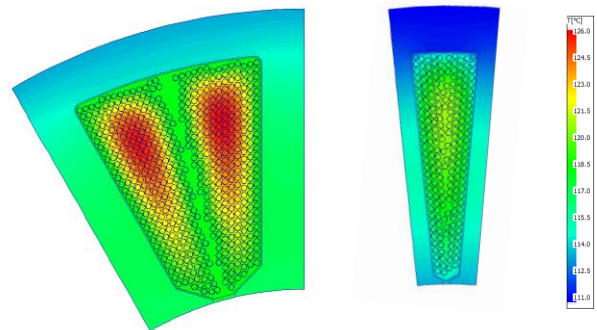


Figure 12. Prediction of heat transfer for 12 slot and 33 slot design

A lumped parameter thermal model has been developed for each design using Motor-CAD [11] and the models have been calibrated based upon the test data from the 12 slot design as well as results from the 2D thermal FEA analysis.

Figs. 13-14 show the thermally constrained operating envelope for each design with a maximum winding hotspot temperature of 170°C. This is calculated by coupling the electromagnetic and loss models to the lumped-parameter thermal model and solving for the maximum winding temperature. In fig. 13 the measured magnet and AC loss components are neglected in the calculation as these are currently unknown for the 33 and 36 slot designs. The 12 slot shows the highest performance envelope due to lower copper and iron losses and the 33 slot slightly outperforms the 36 slot due to a higher fundamental winding factor and marginally lower iron loss. Fig. 15 shows the 12 slot design with the additional measured magnet and AC loss components included into the model. This has a dramatic effect on the envelope with a 42% reduction in continuous output power at maximum speed. If these stray rotor loss components are reduced in the distributed winding designs then the difference in performance between the concentrated and distributed winding topologies may be decreased.

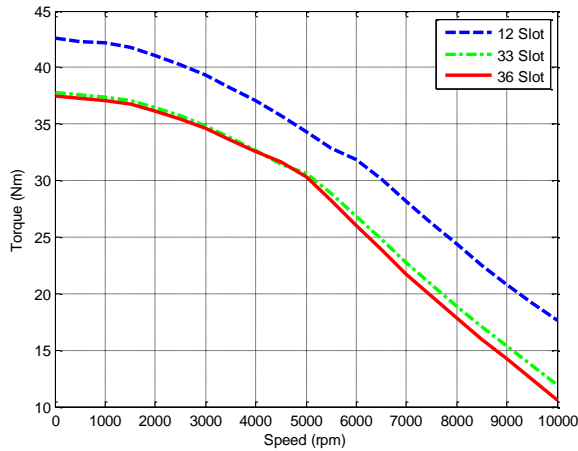


Figure 13. Thermally constrained maximum continuous torque envelope for all designs

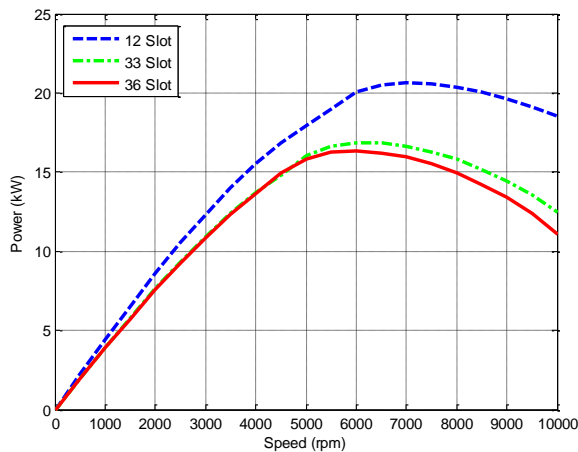


Figure 14. Thermally constrained maximum continuous power envelope for all designs

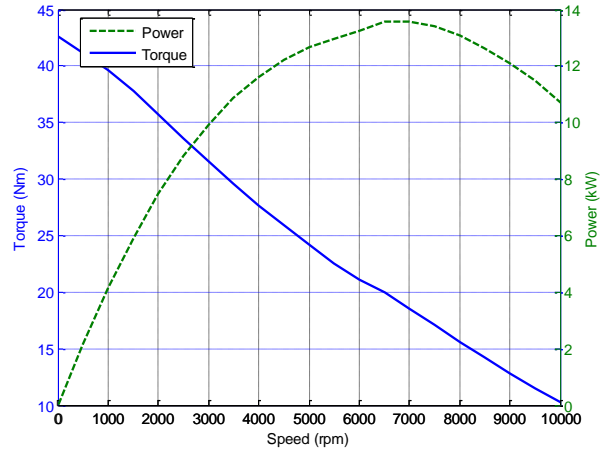


Figure 15. Thermally constrained continuous operating envelope for the 12 slot design with measured rotor and ac loss included

VI. COGGING TORQUE AND TORQUE RIPPLE AND ACOUSTIC NOISE

The cogging torque and torque ripple has been calculated for each design using FEA and is shown in table VII. The cogging torque in the 12 slot is much larger than the distributed designs in which the cogging torque is very close to zero. However when the on load torque ripple is analysed the difference is lower with only slightly reduced torque ripple from the 33 slot design when compared to the 12 slot. The 36 slot topology gives the smoothest calculated torque profile.

TABLE VII-COGGING TORQUE AND TORQUE RIPPLE

	12 Slot	33 Slot	36 Slot
Pk-Pk Cogging Torque (Nm)	0.75	0.01	0.01
Torque ripple at rated torque (%)	5.55	5.23	3.53

Acoustic noise and vibration is found to be high in 12 slot 10 pole combinations [5] due to radial forces generated from the interaction between the permanent magnet airgap field and the stator mmf field. This results in a radial force density waveform with large 2nd, 10th and 12th order spatial harmonic components. Typically the lowest vibration mode is most critical as the radiated acoustic noise associated with higher order vibration modes will be low due to the mechanical stiffness of the stator [12]. During on load testing and at short circuit the 12 slot 10 pole design was found to emit a significant amount of acoustic noise above 3000rpm. From measurements of the noise the 10th spatial harmonic, twice the electrical frequency, was found to be dominant however a significant increase in the level of noise and vibration was observed between open circuit and on-load conditions. This suggests that the predicted 2nd

harmonic resulting from the interaction between the PM field and stator mmf contributes to the noise and vibration during on-load operation. This low order harmonic would not be present in the 33 slot and 36 slot designs and may make the distributed winding machines more appropriate for use in an electrical vehicle application.

VII. CONCLUSIONS

A comparison has been undertaken between a 36 slot, 33 slot and 12 slot, 10 pole IPM motor each with an identical rotors. It is found that the 12 slot design has the highest inductance which in this application gives improved field weakening at rated current but gives the lowest peak power within a given inverter limit and the smallest saliency ratio. The electromagnetic performance of the 33 and 36 slot designs are similar, the 33 slot 10 pole combination has the highest fundamental winding factor which slightly improves torque production however the unbalanced magnetic pull associated with the 33 slot 10 pole design may result in increased mechanical loss and vibration. A sinusoidal back-emf waveform with low harmonic distortion is achieved for all the slot/pole combinations.

On paper the 12 slot concentrated winding is found to produce the lowest copper and iron loss however during testing a significant amount of additional rotor power loss was identified during short circuit and on-load tests. Thermally the distributed windings give better heat transfer through the slots which partly mitigate the additional copper and iron losses. All the designs give a reasonably low level of torque ripple and the 12 slot 10 pole topology is found to emit a significant amount of acoustic noise during on-load and short circuit tests.

VIII. ACKNOWLEDGEMENT

Thanks to Dr. Jason Yon and Dr. Niall Oswald at the University of Bristol and Dr. Tim Allen at Tirius Ltd.

This work was supported by the Bristol University EPSRC funded Industrial Doctorate Centre in Systems (Grant EP/G037353/1) and Motor Design Ltd

IX. REFERENCES

[1] A. M. EL-Refai, "Fractional-Slot Concentrated-Windings Synchronous Permanent Magnet Machines: Opportunities and Challenges," *IEEE Transactions on Industrial Electronics*, vol. 57, no. 1, pp. 107–121, Jan. 2010.

[2] A. M. EL-Refai and T. M. Jahns, "Optimal Flux Weakening in Surface PM Machines Using Fractional-Slot Concentrated Windings," *IEEE*

Transactions on Industry Applications, vol. 41, no. 3, pp. 790–800, May 2005.

[3] L. Chong, R. Dutta, N. Q. Dai, M. F. Rahman, and H. Lovatt, "Comparison of concentrated and distributed windings in an IPM machine for field weakening applications," in *Universities Power Engineering Conference (AUPEC)*, 2010, pp. 1–5.

[4] Z. Q. Zhu, Z. P. Xia, L. J. Wu, and G. W. Jewell, "Analytical Modeling and Finite-Element Computation of Radial Vibration Force in Fractional-Slot Permanent-Magnet Brushless Machines," *IEEE Transactions on Industry Applications*, vol. 46, no. 5, pp. 1908–1918, Sep. 2010.

[5] G. Dajaku and D. Gerling, "Magnetic radial force density of the PM machine with 12-teeth/10-poles winding topology," in *2009 IEEE International Electric Machines and Drives Conference*, 2009, pp. 1715–1720.

[6] F. Magnussen and C. Sadarangani, "Winding factors and Joule losses of permanent magnet machines with concentrated windings," in *IEEE International Electric Machines and Drives Conference, 2003. IEMDC'03.*, 2003, vol. 1, pp. 333–339.

[7] R. Wrobel and P. H. Mellor, "Design considerations of a direct drive brushless PM machine with concentrated windings," in *IEEE International Conference on Electric Machines and Drives, 2005.*, 2005, pp. 655–658.

[8] Z. Li and A. Miotto, "Concentrated-winding fractional-slot synchronous surface PM motor design based on efficiency map for in-wheel application of electric vehicle," in *2011 IEEE Vehicle Power and Propulsion Conference*, 2011, pp. 1–8.

[9] J. Goss, R. Wrobel, P. Mellor, and D. Staton, "The Design of AC Permanent Magnet Motors for Electric Vehicles: A Design Methodology," in *IEEE International Electric Machines and Drives Conference*, 2013.

[10] J. Goss, P. H. Mellor, R. Wrobel, D. A. Staton, and M. Popescu, "The design of AC permanent magnet motors for electric vehicles: a computationally efficient model of the operational envelope," in *6th IET International Conference on Power Electronics, Machines and Drives (PEMD 2012)*, 2012, pp. B21–B21.

[11] Motor Design Ltd., "Motor-CAD v7.5 Software." 2012.

[12] Z. Q. Zhu, Z. P. Xia, L. J. Wu, and G. W. Jewell, "Influence of slot and pole number combination on radial force and vibration modes in fractional slot PM brushless machines having single- and double-layer windings," in *2009 IEEE Energy Conversion Congress and Exposition*, 2009, pp. 3443–3450.